EXPERIMENTAL INVESTIGATION OF ULTRAHIGH VACUUM ADHESION AS RELATED TO THE LUNAR SURFACE

FOURTEENTH QUARTERLY PROGRESS REPORT

1 JANUARY 1968 THROUGH 30 APRIL 1968

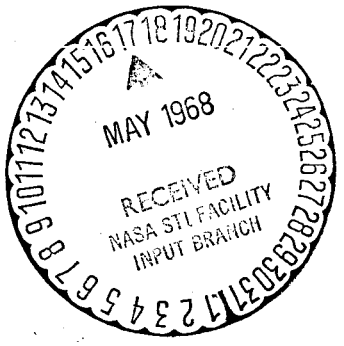

J. A. Ryan
Principal Investigator

J. J. Grossman
Co-Principal Investigator

R&D/Space Sciences Department

Prepared for:
NASA Office of Advanced
Research and Technology
Washington, D. C.

Contract NAS7-307
Date of Issue:
26 June 1964
A-830-BBK3-44

MISSILE & SPACE SYSTEMS DIVISION
DOUGLAS AIRCRAFT COMPANY
SANTA MONICA, CALIFORNIA

TABLE OF CONTENTS

ABSTRACT

This report presents the results of studies, on the ultrahigh vacuum adhesional behavior of silicates, obtained during the period February 1 through April 30, 1968. Work consisted of contacting ultrahigh vacuum cleaved silicate surfaces with argon ion sputtered metal surfaces, and investigation of the mechanisms responsible for the considerable electrostatic charging of silicates produced by ultrahigh vacuum cleavage. It was found that adhesion between the sputtered metal and cleaved silicates did occur, the measured adhesion force being about 10^2 dynes after touch contact. It appears that the primary if not sole contributor to this adhesion is the electrostatic charging of the silicate, but much more work is required to determine the precise effect of metal surface state. The electrostatic charging studies further verified the highly anisotropic nature of the charging. They also demonstrated that massive breakdown in the charge anisotropy occurs as system pressure is increased and that recovery can occur. Photomicrographic study of the cleaved surfaces (before and after defect etching) and electron microprobe analysis reveal a close correlation between the charge and composition gradient profiles. This indicates strongly that the primary contributor to the charging and charge anisotropy in the crystals studied to date is the polarization field associated with the composition gradients.

1.0 INTRODUCTION

1.1 General

This report presents a summary of work accomplished during the period February 1, 1968, through April 30, 1968, on the study of the ultrahigh vacuum adhesional behavior of silicates as related to the lunar surface. This work is being conducted for the Office of Advanced Research and Technology, National Aeronautics and Space Administration, under contract NAS7-307.

1.2 Purposes of Program

The purposes of this program are (a) to obtain quantitative experimental data concerning the ultrahigh vacuum adhesional behavior of silicates in contact with other silicates and with various non-silicates (principally metals), (b) to achieve an understanding of the mechanisms responsible for the observed adhesion, and (c) to investigate techniques for reducing or eliminating the adhesion.

1.3 Approach

The approach used during this report period has been a) to cleave silicates at ultrahigh vacuum and contact these with contaminated, sputtered, and mechanically abraded metal surfaces, (b) to measure the surface distribution of electrostatic charge produced by ultrahigh vacuum cleavage of silicates, and (c) to obtain microchemical and microphysical profiles of vacuum-cleaved silicate surfaces. Approach (a) serves to provide information concerning the adhesional behavior of silicates in contact with metals with the various surface states which may be present during lunar missions. Approaches (b) and (c) serve to provide information concerning the mechanisms which may be responsible for the observed surface charging.

2.0 EXPERIMENTAL RESULTS

2.1 Silicate-Metal Adhesion as a Function of Metal Surface State

Various experimental difficulties were encountered during this quarter which limited the amount of silicate-metal adhesional data obtained. First a succession of leaks developed in the vacuum system. Each leak caused the loss of approximately one week experimental time. Second, various problems were found with the sputtering technique. One was related to the system geometry in that arcing occurred from the high voltage lead. This was eliminated by improving the insulation and separating the lead further from areas at ground potential. Another problem was that the silicate sample tended to become coated with sputtered material. Once this occurred sufficient current would flow through the sample hangdown wire to cause it to melt (and hence fail). This problem was resolved by shielding the sample completely from the discharge.

Three runs were made during the quarter, all for microcline (001) contacting commercial aluminum 2024.

Runs #1 and 2

The system was evacuated to 3×10^{-10} torr, then backfilled to 15 microns with purified argon. The metal sample was then sputtered for about 10 minutes at 400 ma current. The microcline was then cleaved and contacted with the sputtered aluminum (at a system pressure of 15 microns argon) 15 minutes after sputtering and about 5 minutes after cleaving. No adhesion was detected.

Run #3

The system was evacuated to 2×10^{-10} torr then backfilled to 15 microns with argon. The metal sample was sputtered for 15 minutes at 400 ma. Following sputtering, the ion pump was turned on. The microcline was cleaved five minutes after sputtering at a system pressure of 5×10^{-8} torr. First contact was made four minutes after cleavage. An adhesion force of about 3×10^{2} dynes was measured after touch contact. This decreased within three minutes to 1×10^{2} dynes and the force remained at this level for 3 1/2 hours at which time the run was terminated. No long range force was detected. However, sputtered material was deposited on the viewport making it difficult to see the sample so it is not certain whether or not some long range attraction might have been present.

2.2 Electrostatic Charging

During this quarter, the electrometer probe has been redesigned so that the electrostatic charge distribution can be measured more accurately and with less ambiguity than at present. The new electrometer probe will penetrate a guard plane consisting of a partially transparent electrode deposited on a glass flat. This electrode will have negligible resistance for the electrometer circuit yet provide a window for positioning the probe relative to the crystal surface. Since the effective probe area is hence decreased relative to the one being used now, the Keithley Model 610B electrometer will be replaced by a Keithley Model 640 Electrometer because it has three orders of magnitude greater sensitivity.

The electrometer arm is being shortened several centimeters by rearranging one of the crosses in the assembly. This should reduce mechanical variations in the probe-crystal distance which seem to be one factor in an observed apparent random fluctuation of charge with time.

Two runs were completed during this quarter (#2 and #3) and a third (#4) is in progress. These runs were performed using a single orthoclase cylinder having three cleavage notches oriented so that the effect of cleavage direction could be studied. In addition, further out-of-chamber work was done on the sample utilized in Run #1.

Run #1:

Figure 1 is a composite photograph showing the cleavage behavior of the orthoclase crystal [along the (001) plane]. The cleavage starts at the midpoint of the cleavage notch (top of photograph), radiates rapidly towards the sample edge followed by the main cleavage along the b-axis. Figure 2a is an

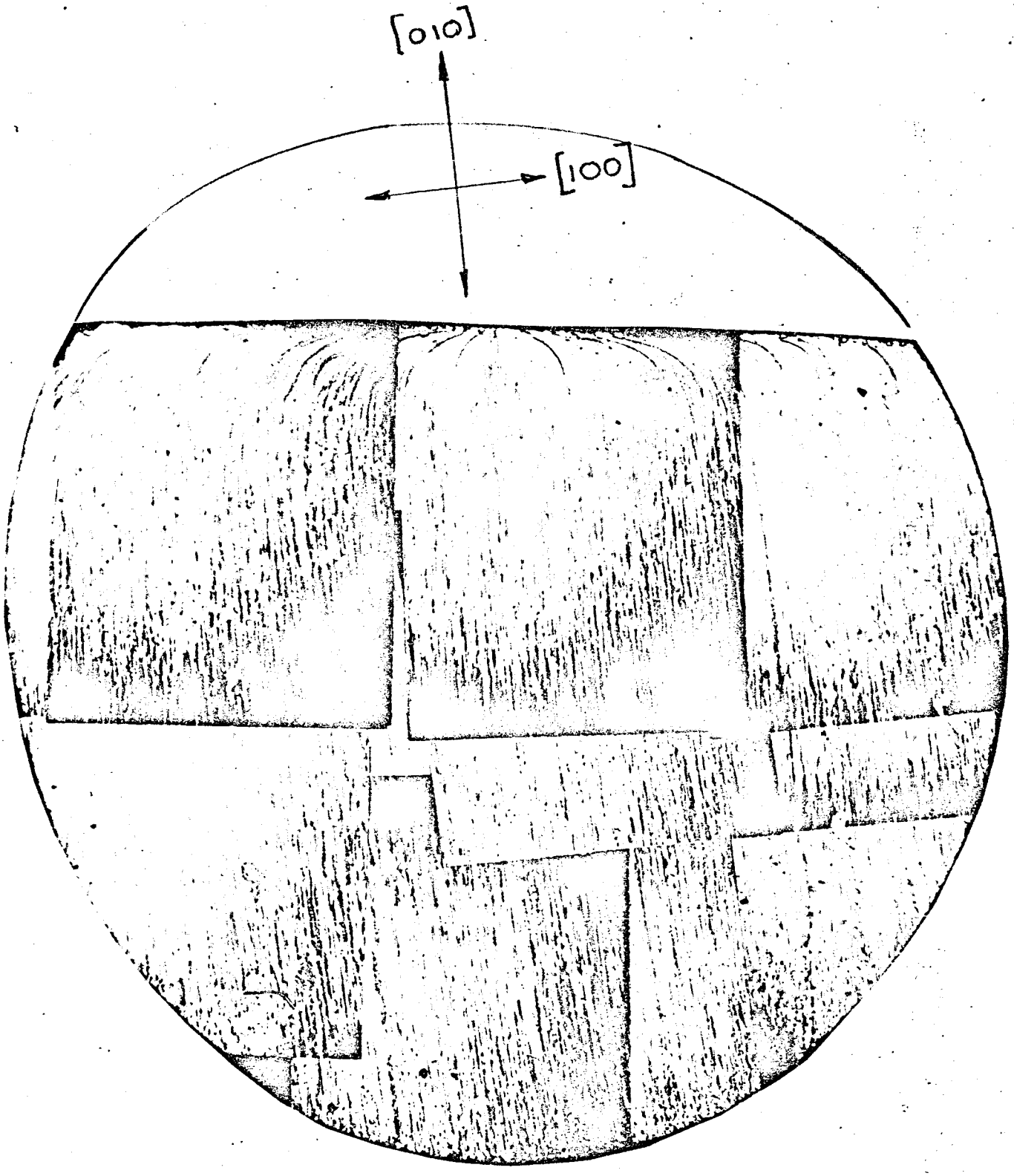

Figure 1. Composite photomicrograph of the (001) cleavage surface of orthoclase, Run #1.

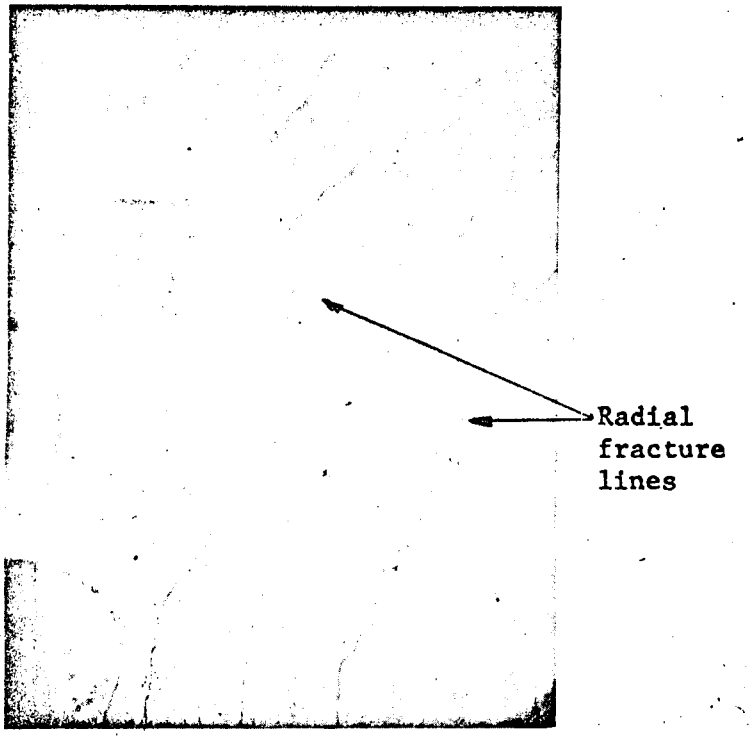

(a)

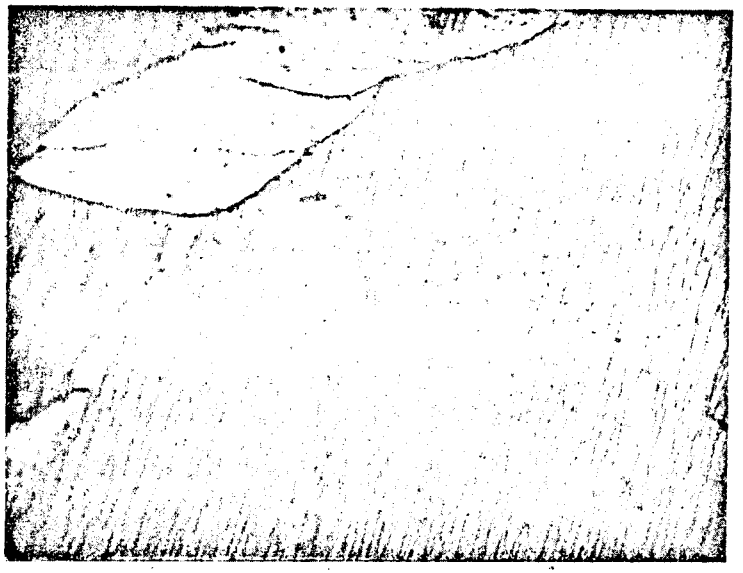

(b) [010]

Figure 2. Phase contrast photomicrographs near cleavage notch, Run #1. (a) Magnification 500x; (b) etched surface, magnification 333x

enlargement near the upper edge showing how the cleavage direction rotates towards the direction of the b-axis. The microperthite structure of the orthoclase is clearly visible as a refractive index change. Figure 2b is the same area after acid etching and Figures 3a and 3b are electron photomicrographic replicas of aluminized surfaces after etching which show the perthite structure in slightly greater detail. Electron microprobe analysis of the elemental distribution in the orthoclase sample (along the cleavage surface) was carried out. Two techniques were utilized. First, using a 2 micron beam diameter (nominally smaller), step traces at 1 micron intervals were taken of various combinations of three elements simultaneously. These are shown in Figure 4 through 7. Second, using a 50 micron beam diameter, an array of points, 500 microns apart, covering the entire surface of the crystal was used to map the composition distribution. Distributions for potassium and silicon are shown in Figures 8 and 9 respectively.

The microperthite analyses, Figures 4 to 7, show that the etched regions in the Figure 3 electron photomicrographs, are albite (Na, Ca rich) exsolution regions in an orthoclase (K, Ba rich) host crystal. Figure 4 shows that the K and Ca compositions vary anticoincidently, whereas Figure 5 shows that the K and Ba concentrations vary coincidently. Figure 6 shows that Na varys in the same direction as Ca but oppositely to Ba. Figure 7 completes the series showing potassium and sodium vary in opposite directions. The sharp phase boundaries in the electron photomicrographs where the transition zone is less than 0.3 microns suggest that the electron microprobe beam is averaging the sample both laterally as well as by the depth of penetration.

The large area array, Figures 8 and 9, gives the average composition since the 50 micron beam diameter is a reasonably good average over the microstructural

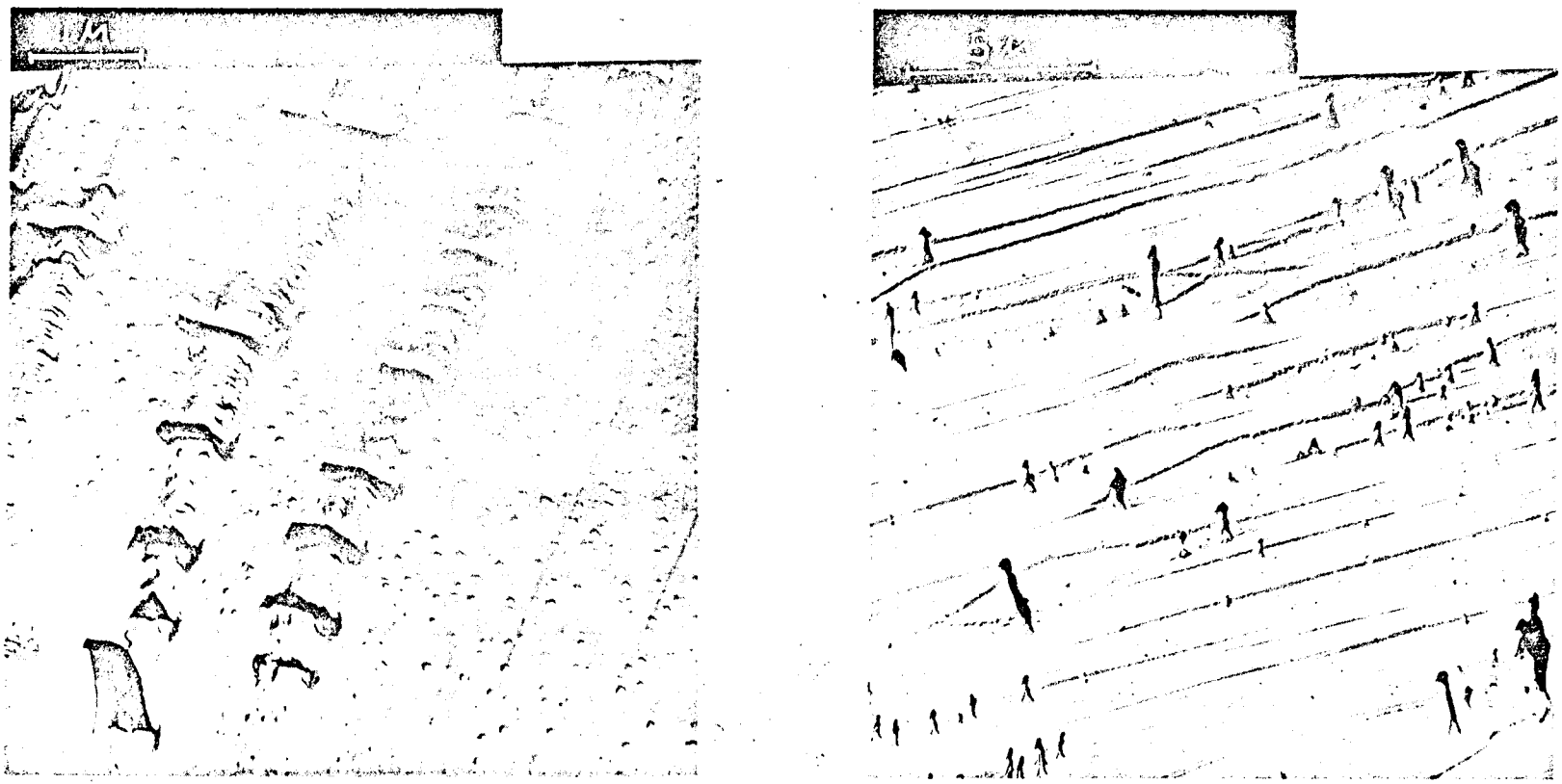

Figure 3. Electron photo-micrographs of replicas of the vacuum aluminized (001) cleavage surface of orthoclase, Run #1, showing the perthite and defect structure developed by chemical etching.

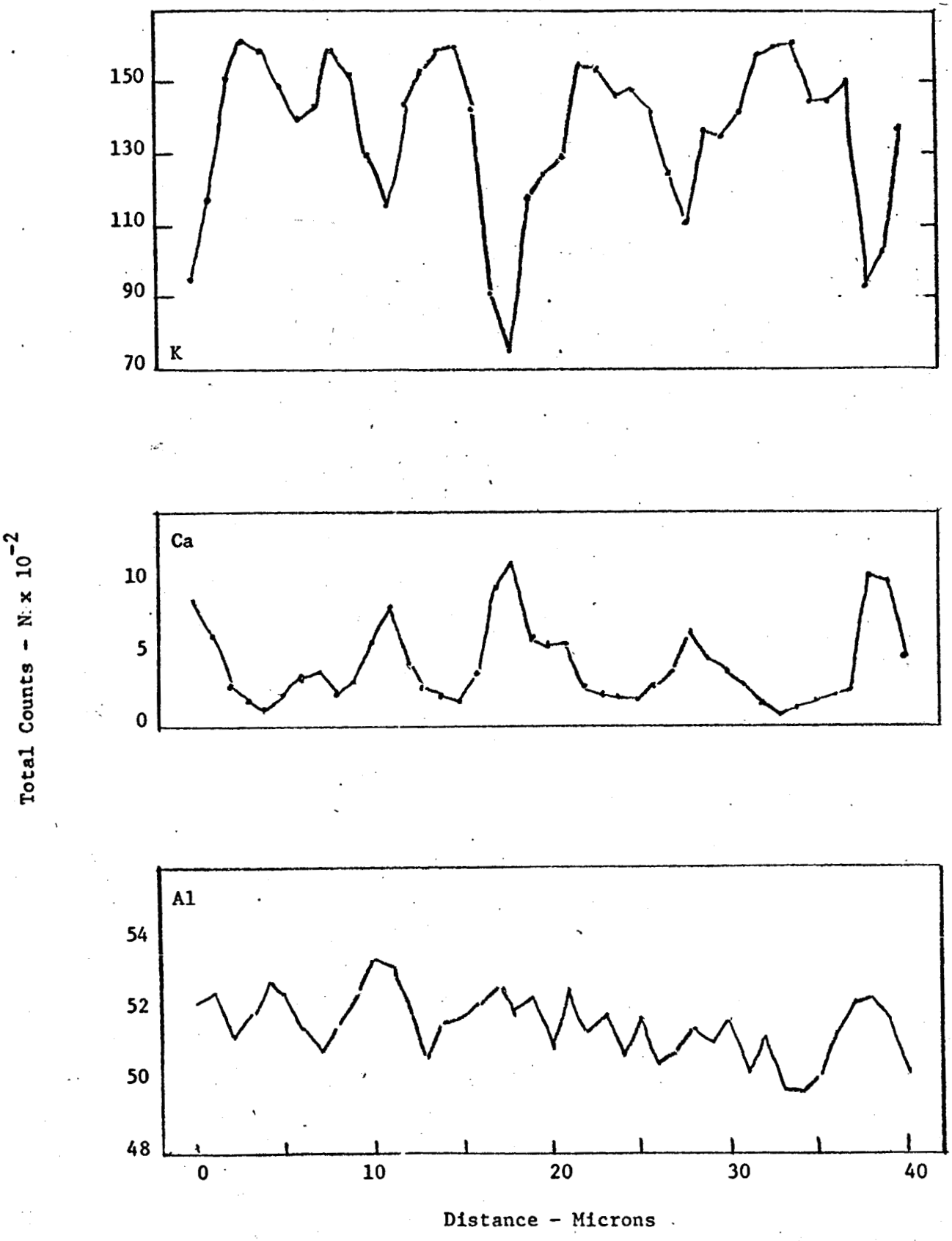

Figure 4. Step scan electron microprobe analysis of the orthoclase microperthite structure in Run #1 for potassium, calcium and aluminum

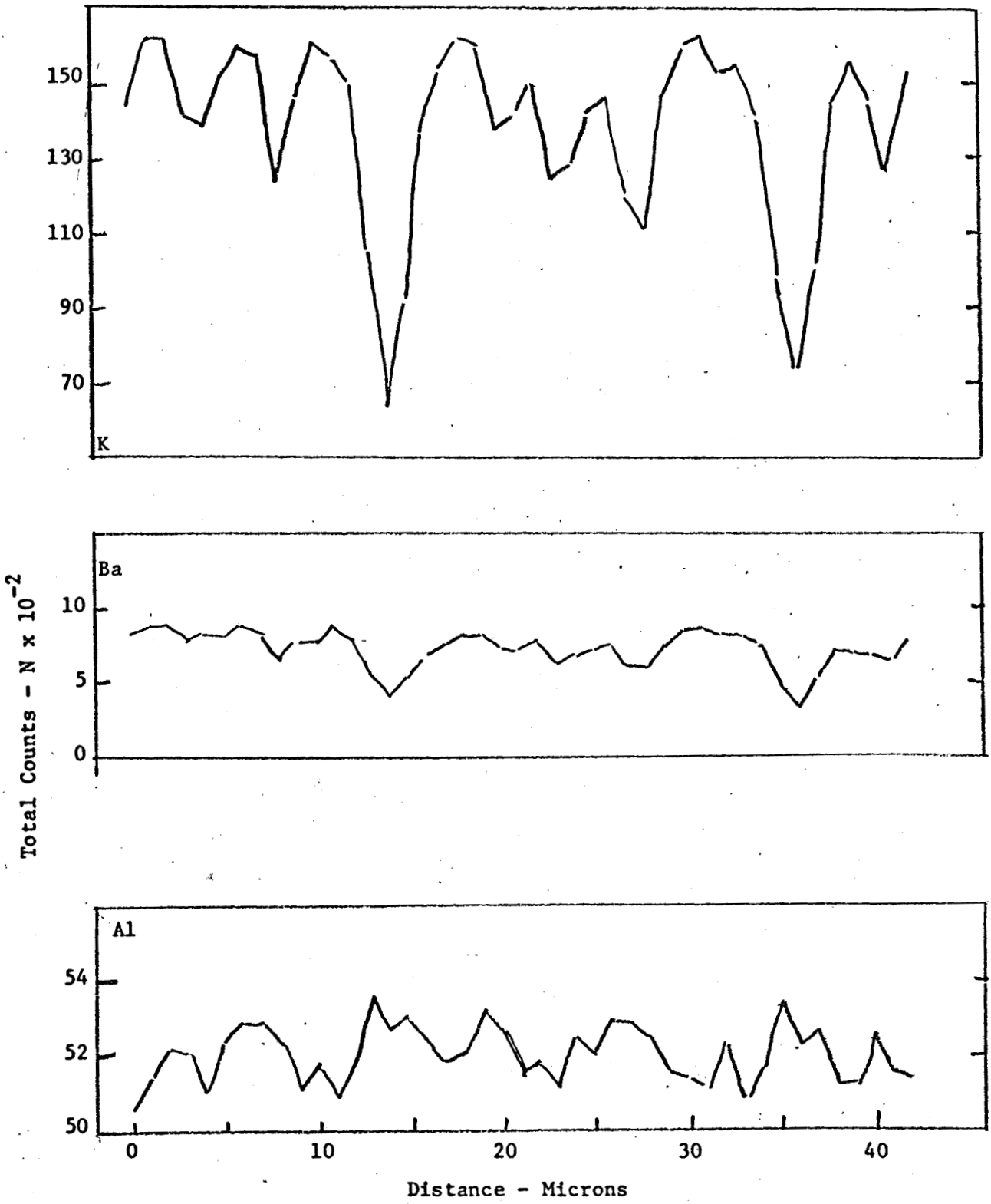

Figure 5. Step scan electron microprobe analysis of the orthoclase microperthite structure in Run #1 for potassium, barium and aluminum.

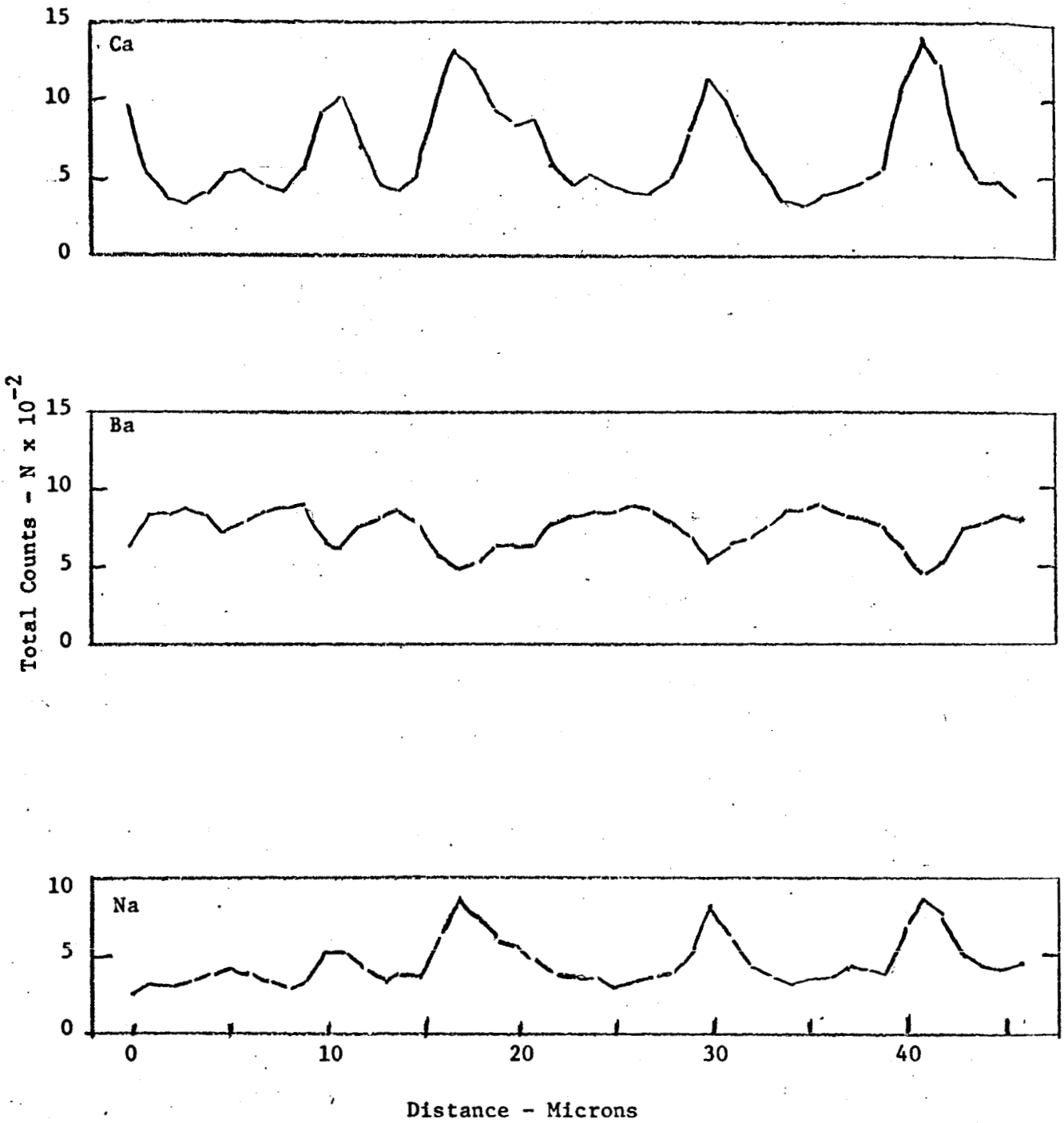

Figure 6. Step scan electron microprobe analysis of the orthoclase microperthite structure in Run #1 for calcium, barium and sodium.

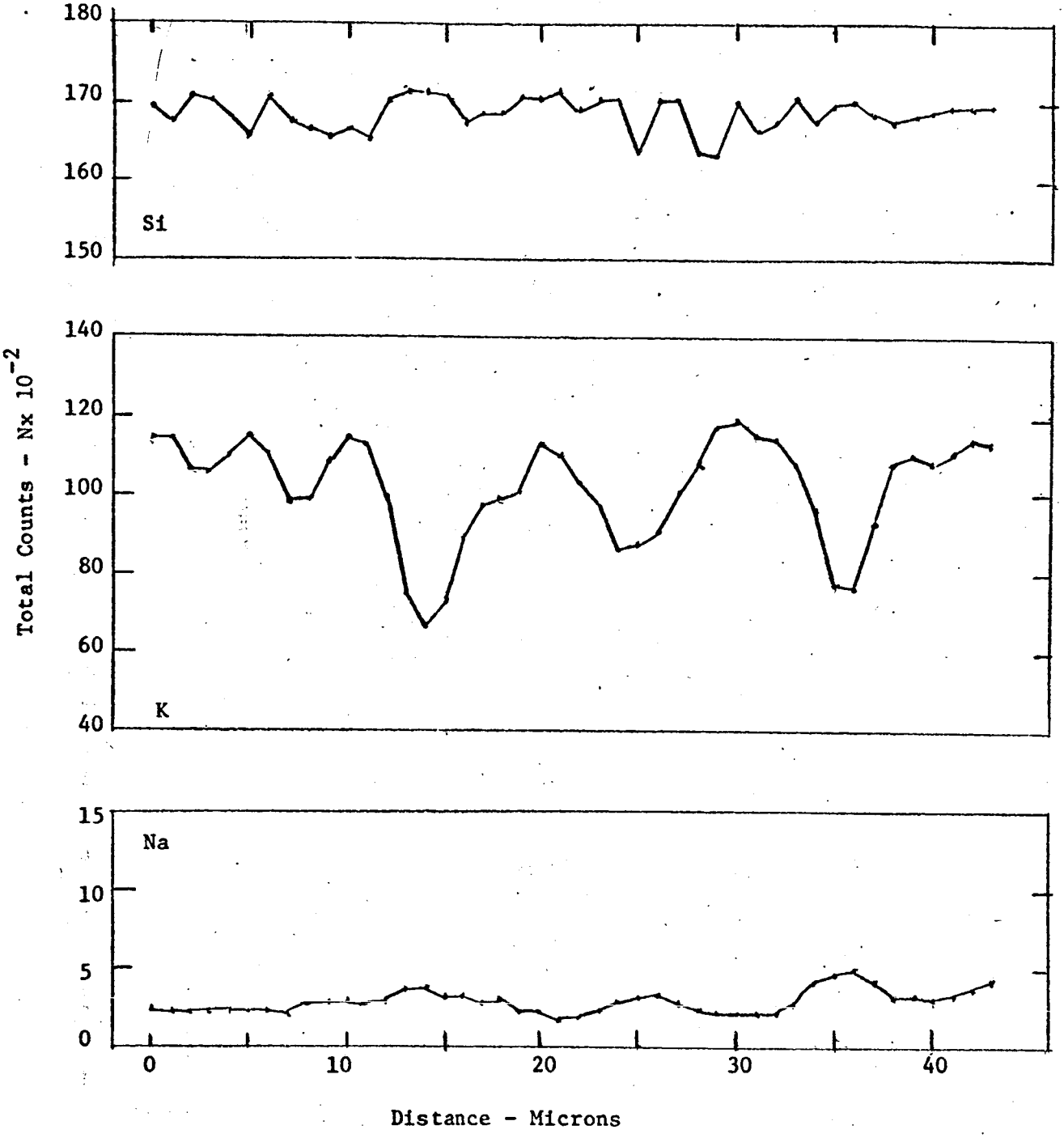

Figure 7. Step scan electron microprobe analysis of the orthoclase microperthite structure in Run #1 for silicon, potassium and sodium.

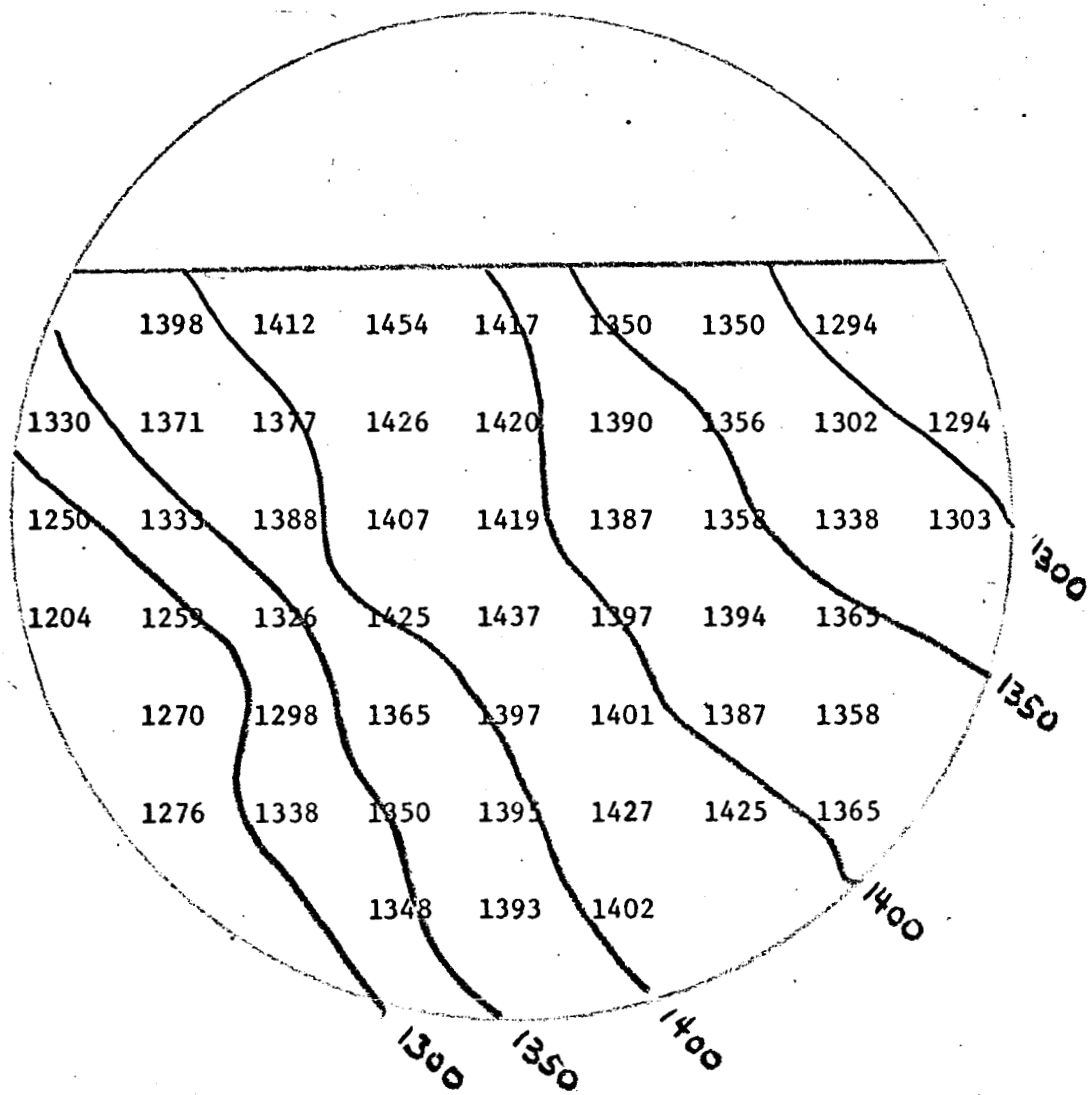

Figure 8. Distribution of potassium on or thoclase (001) surface, Run #1, using 50 micron beam diameter. Points are spaced 500 microns apart.

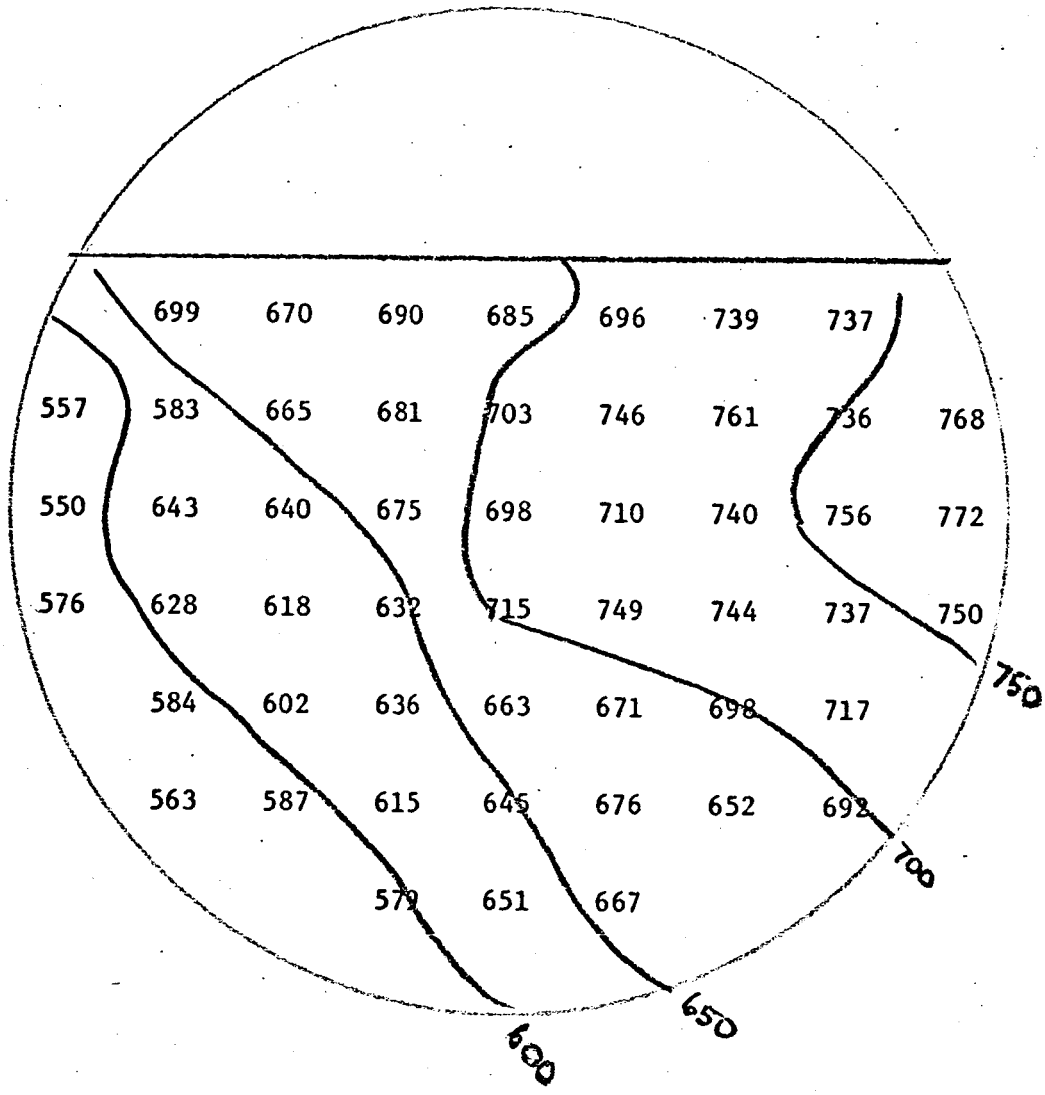

Figure 9. Distribution of silicon on or thoclase (001) surface, Run #1, using 50 micron beam diameter. Points are spaced 500 microns apart.

elements which are less than 8 microns wide. From these arrays, the composition is found to very over the surface of the crystal with the lines of constant composition oriented almost along the b direction (see Figure 1).

Run #2

In the last quarterly report, the behavior of the charge distribution for this run was presented from the time of cleavage on 3 January 1968 through the end of the reporting period (30 January). On 6 February 1968, the system was backfilled with dry N_2 and the pressure in the system was raised to 0.35 torr. Two discharge pulses were observed, the first at 0.16 torr and the second at 0.33 torr. The charge distributions are shown superimposed in Figure 10, and the location of the probe when discharge occurred is also indicated. An order of magnitude decrease in the charge as well as a major modification in the distribution are observed. The first discharge reduced the peaks almost uniformly whereas the second discharge produced a distinct dip at the point of discharge on the crystal face. This is probably due to discharge near the edge of the notch, Figure 11.

The system was then re-evacuated to 10^{-9} torr. A redistribution of charge was then observed as well as some recovery in the overall difference between the maximum peak and valley in the charge distribution. This recovery, a twofold increase over that remaining at 0.35 torr, is shown in Figure 12. The redistributed charge is compared to the original charge distribution in Figure 13. The effect of the second discharge at 0.33 torr persists as seen both in Figure 10 and 13.

On 7 February 1968, the sample was again discharged by admitting dry N_2 to the vacuum system. Table 1 summarizes the discharge history on both days.

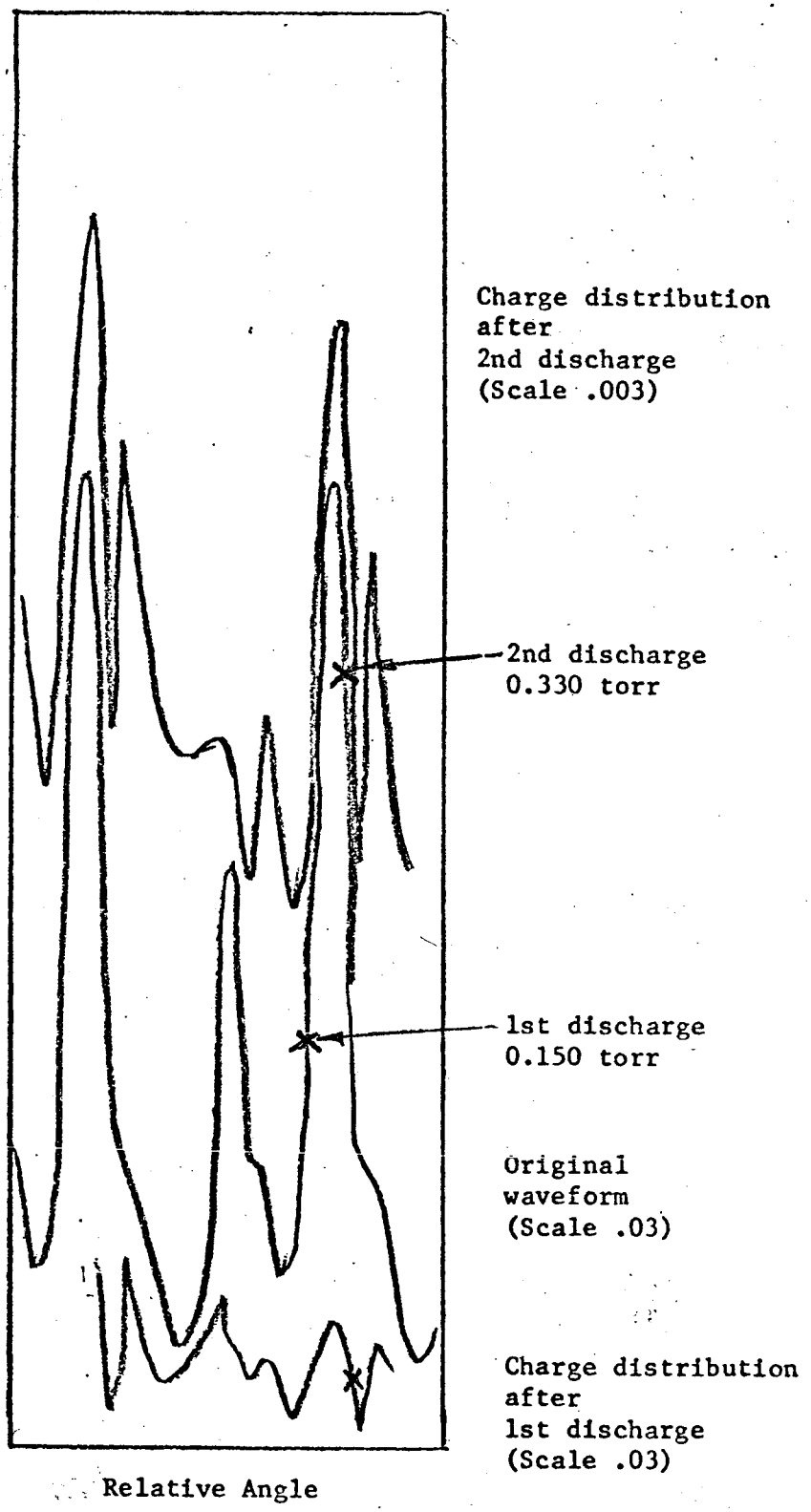

Figure 10. Comparison of charge distributions before and after first two discharges, Run #2, 6 Feb. 1968.

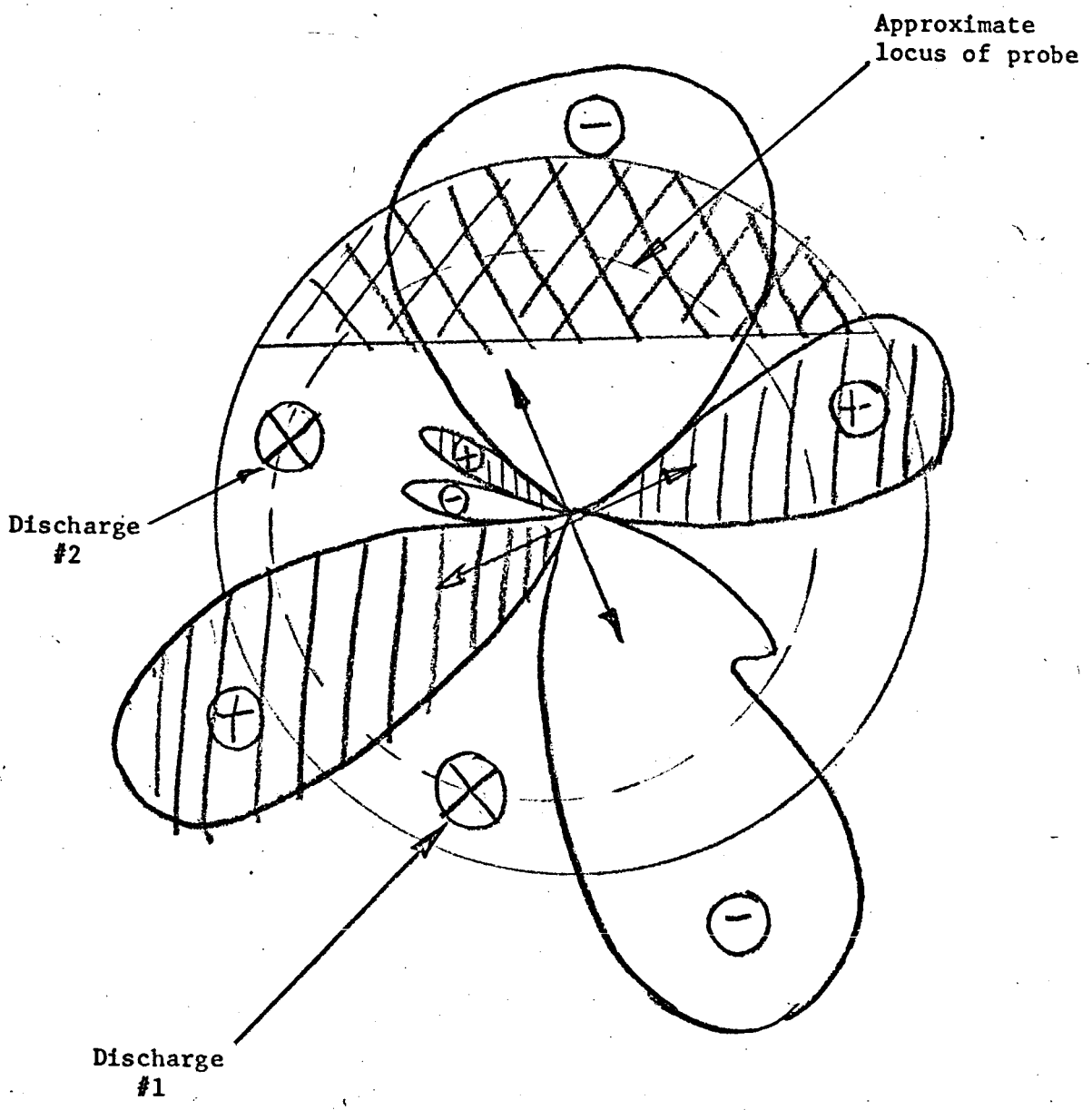

Figure 11. Schematic drawing of discharge configuration and the resulting charge distribution lobe pattern, Run #2. The approximate orientation of the crystal axis is shown. These will be determined accurately when removed from the vacuum system at the end of Run 4.

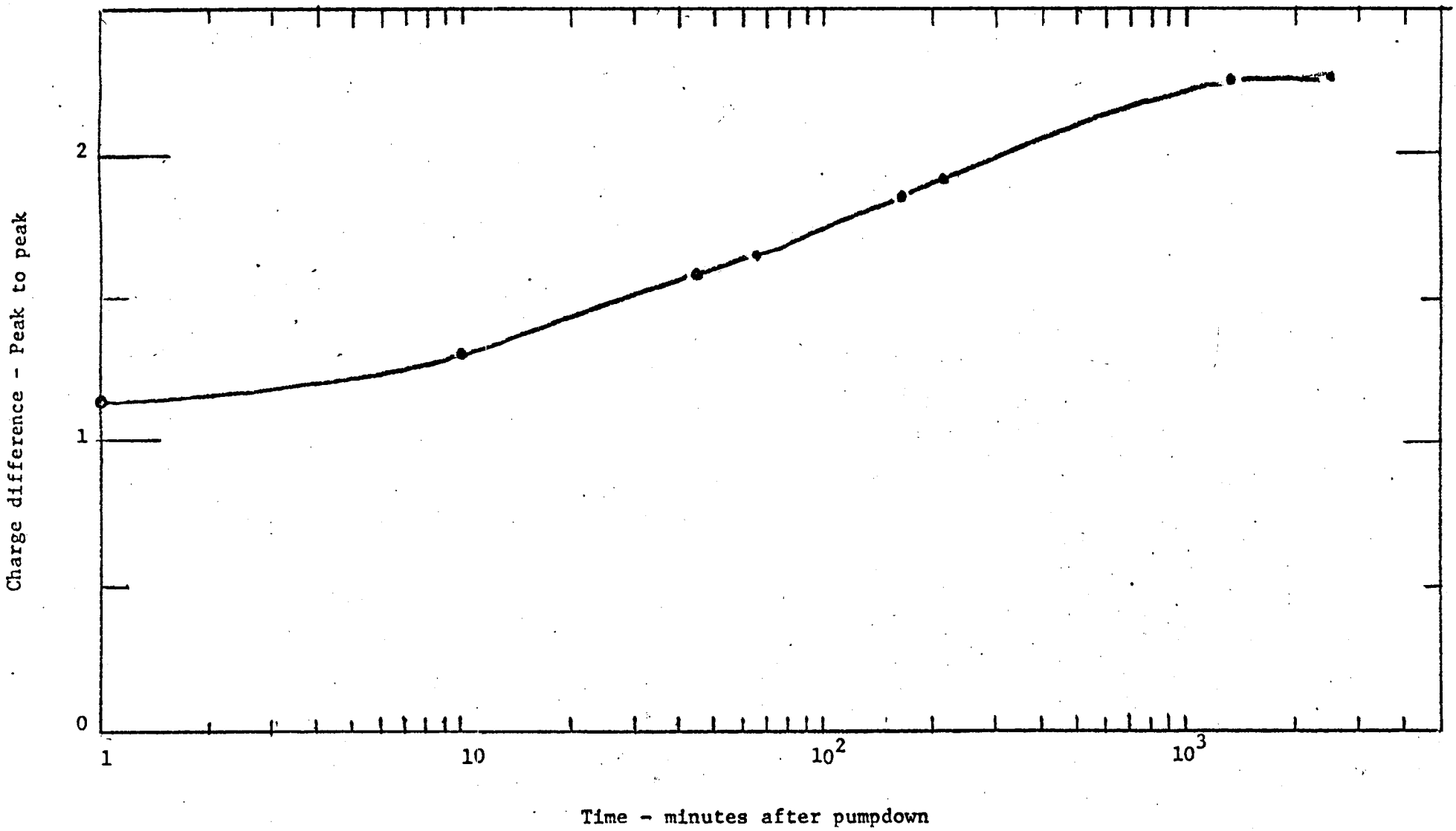

Figure 12. Recovery of charge distribution assymetry at 10^{-9} torr after discharge in dry nitrogen at 0.360 torr, Run #2.

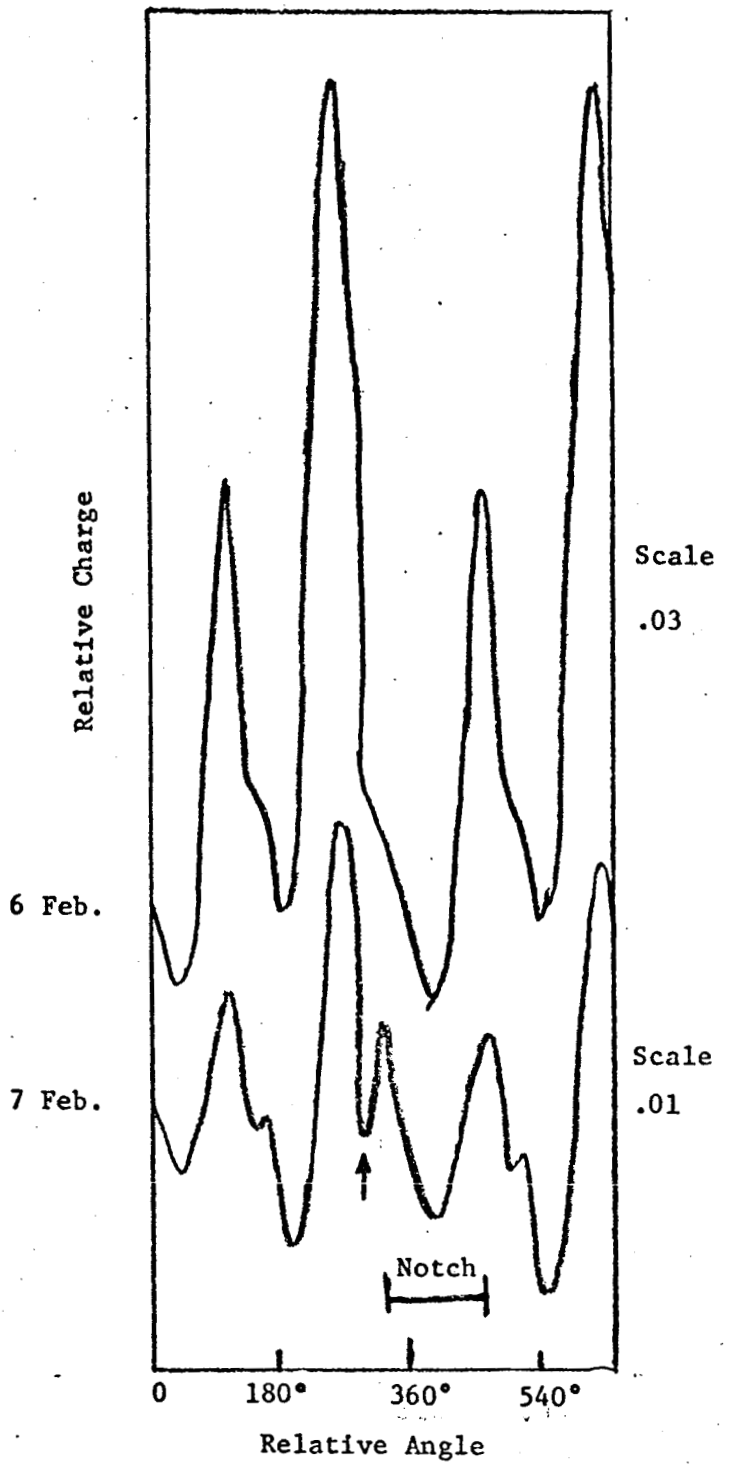

Figure 13. Comparison of charge distribution before discharge and after recovery, Run #2. Relative orientation of notch is shown together with discharge pulse at 290°. Note scale change. Amplitude before discharge over 5x greater than afterwards.

TABLE I

Pressure at Which Discharge Occurred and Relative Magnitude of Discharge: Run #2

Date	Pressure at Discharge (torr)	ΔQ of Probe (Conlombs)
6 Feb 68	0.16	$> + 10^{-12}$ *
	0.33	$> + 10^{-12}$ *
7 Feb 68	0.43	$+ 21.5 \times 10^{-12}$
	0.58	$> + 10^{-12}$ *
	0.84	$> + 10^{-12}$ *
	1.30	$+ 7.7 \times 10^{-12}$
	1.61	$+ 6.0 \times 10^{-12}$
	2.55	$+ 1.4 \times 10^{-12}$
	1 atmos	None

* Too sensitive a scale, off-scale.

Altogether, a series of eight discharge pulses were observed between 0.16 torr and 2.55 torr. The total charge collected by the probe decreased with each successive pulse.

Run #3

This run represented the second cleavage of the orthoclase crystal used in Run #2. Cleavage was done on 19 February 1968 at a pressure of 1.2×10^{-9} torr. The cleavage notch was oriented at 45° to that in the previous run, as shown in Figure 14.

The charge distributions for both runs were found to coincide when corrected for the angular position of the probe (note that the notch position in Run #3 is such to eliminate the 135° positive lobe found in Run #2).

After cleavage, the difference between the maximum peak and valley charge decayed relatively slowly, Figure 15. Compared to Run #2, which was cleaved at one tenth the pressure, it is seen that the initial rapid decay (of Run #2) is absent, strengthening the hypothesis that gas adsorption is responsible for the fast decay. The existance of an intermediate decay rate, found to have a half-life of 3.5 hours in Run #2, was found again in Run #3 with a 7.2 hour half life. The subsequent behavior of the charge decay rate was similar to Run #2.

On 20 February 1968, in attempting to move the mechanical probe into position to measure the vector field, the electrometer probe inadvertantly scraped the surface of the crystal. This caused a change in the pattern of the charge (Figure 16). One interpretation of this is that the positive peak was discharged by a transfer of electrons from the probe to the crystal surface.

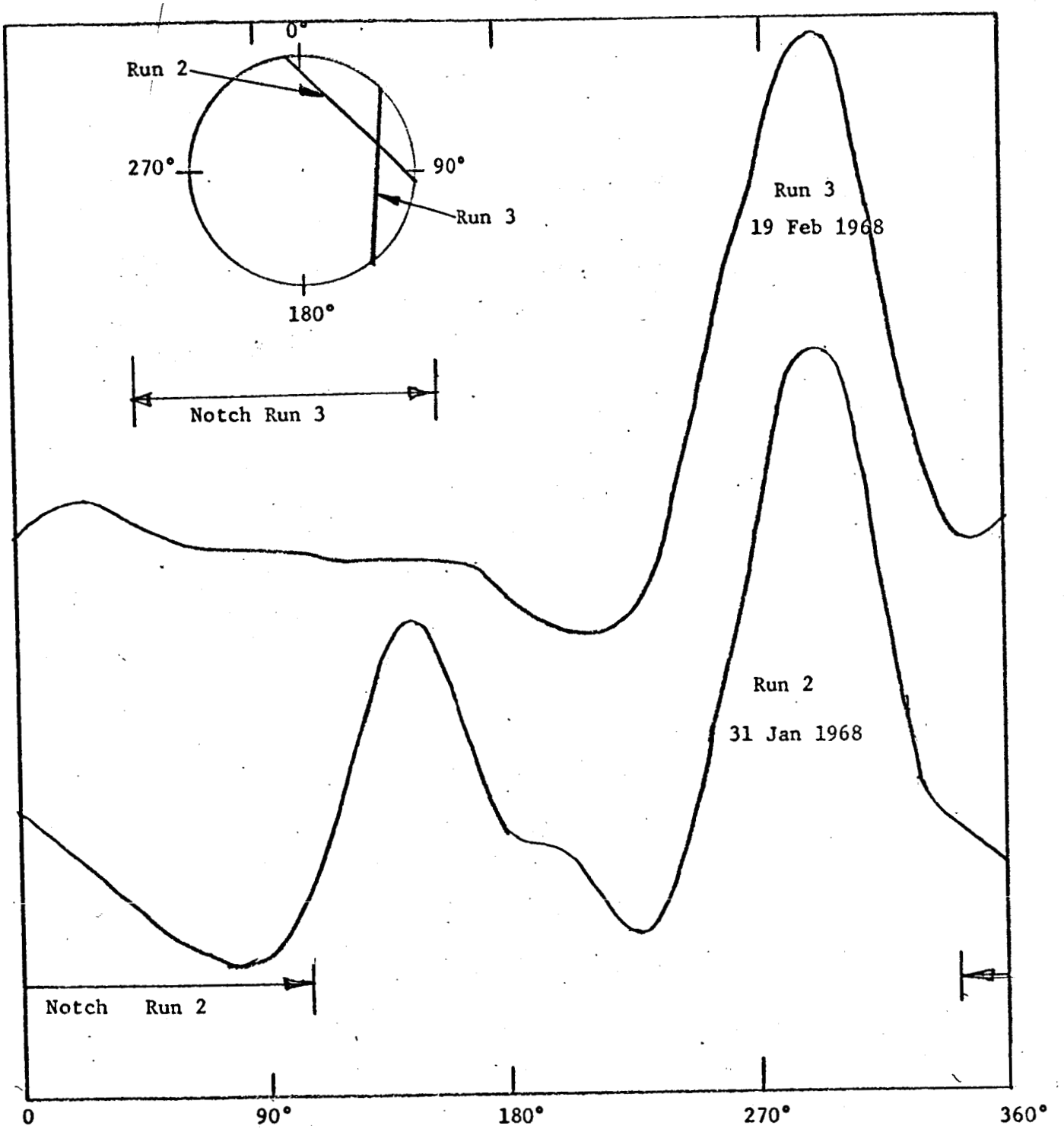

Figure 14. Comparison of charge distributions from Run #2 and Run #3 where cleavages were from two directions 45° apart in the same orthoclase crystal (001) plane. The direction of the B axis will be determined when the samples are removed from the vacuum chamber.

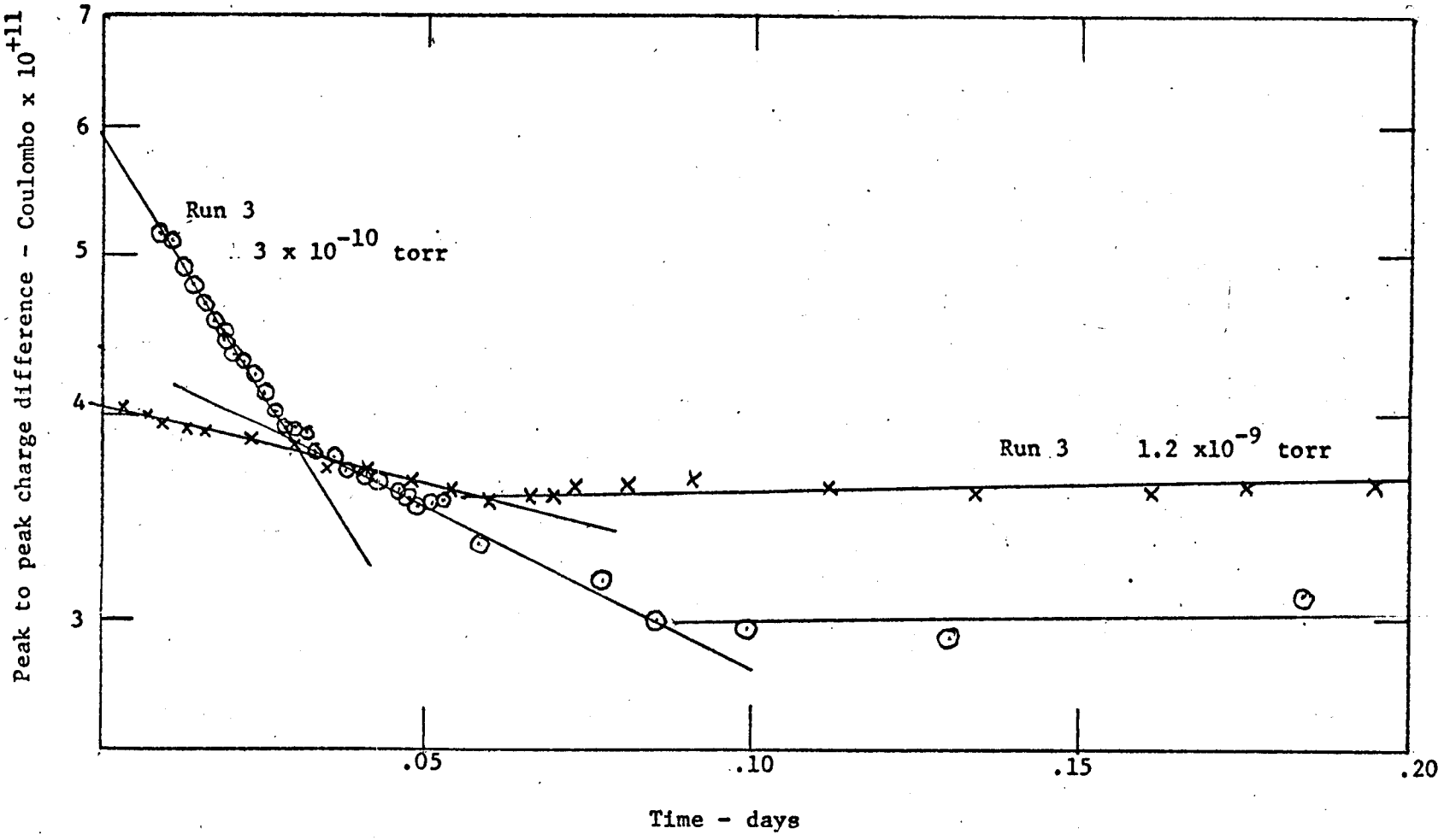

Figure 15. Variation of charge distribution assymetry with time after cleavage at two different pressures. Surface absorption is absent in Run 3 since monomolecular film forms to rapidly to observe.

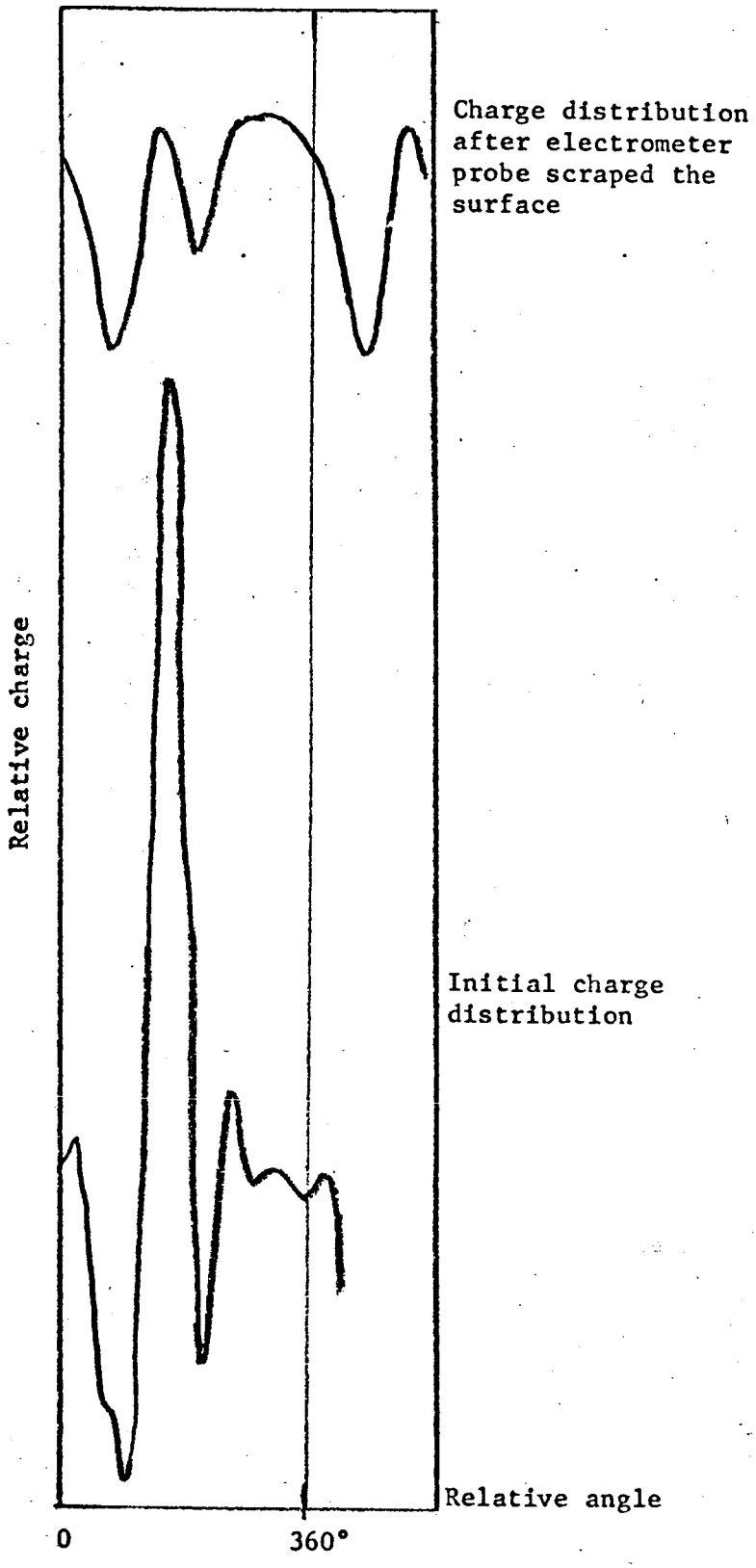

Figure 16. Effect of electrometer probe scraping cleavage surface. The main effect is the decrease in the more positive peak.

After 22 more days the charge asymmetry had been partially restored as shown in Figure 17. The four curves have been made coincident at the base. Since the smaller peak to valley difference remains approximately constant, the charge recovery appears to be a lateral transfer of charge from the maximum peak to the minimum valley.

On 14 March, the system was raised to atmospheric pressure with dry nitrogen. At 36 millitorr, the electrometer probe began drawing a positive current which reached as high as 15 times the electrometer tube grid current of 10^{-14} amps. This effect may also be interpreted as due to small charge pulses at specific crystal orientations (the crystal was being rotated at a constant rate during this period). The major effect is shown in Figure 18. The large negative peak becomes smaller, the positive peak increases a small amount and the middle peaks remain unchanged. After the first large discharge pulse occurred, a general decrease in the charge distribution was observed, the positive peak experiencing a smaller percentage decrease than the negative peaks.

Massive discharges were observed at 0.148 torr, 0.250 torr, 0.360 torr, 0.470 torr together with three smaller pulses between 0.470 and 1.0 torr, and one or two above 1.0 torr. It is interesting to note (Figure 19) that the charge distribution after the second and third discharges was practically identical (except for the scale factor) to the original distribution just after cleavage and prior to the inadvertant scraping of the crystal surface with the electrometer probe.

3.0 DISCUSSION

3.1 Silicate-Metal Adhesion as a Function of Metal Surface State

The first two runs, for which no adhesion was detected, were made at a

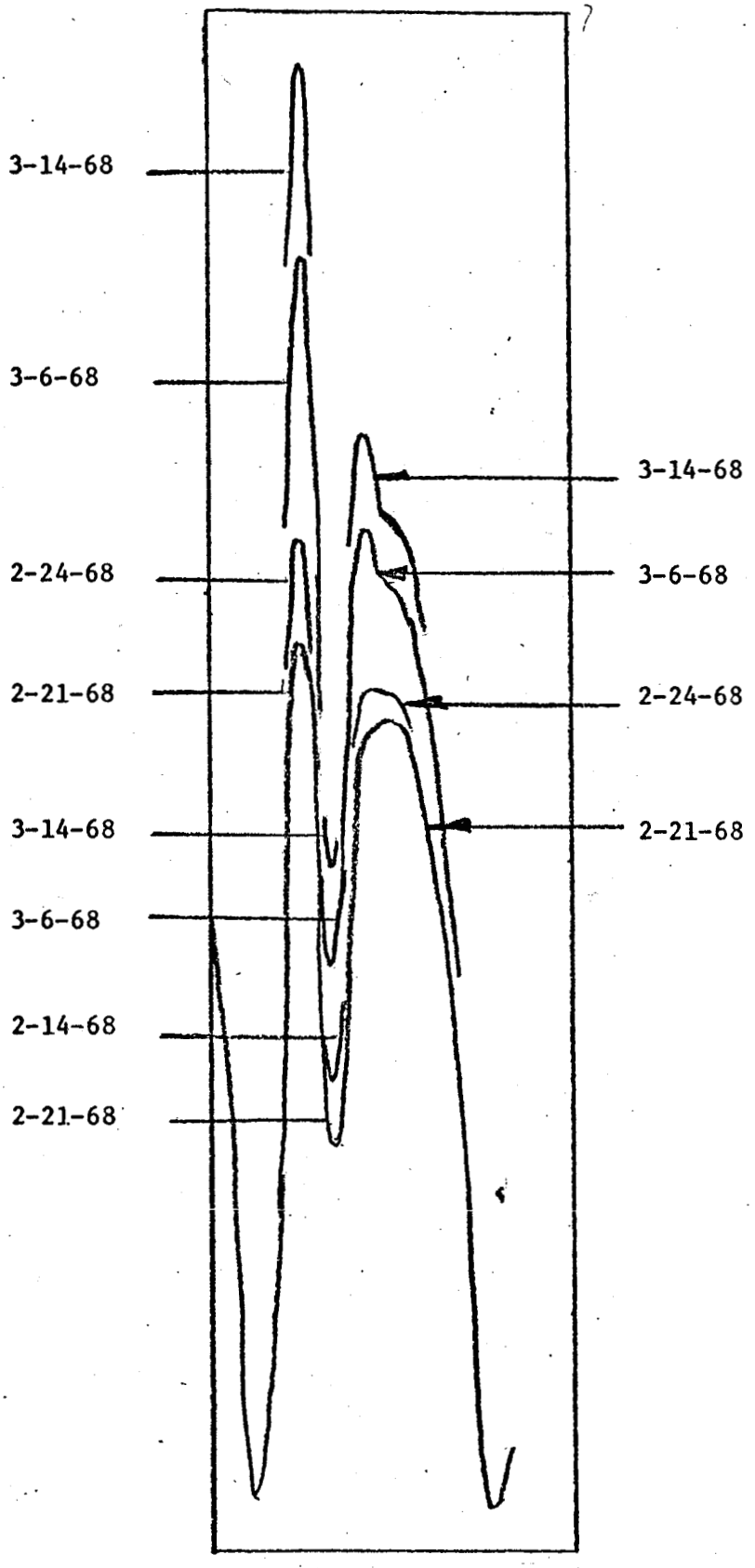

Figure 17. Recovery of charge distribution assymetry after surface was partially discharged when contacted with the electrometer probe, Run #3. The curves were superimposed so that they were coincident at the base. The smaller peak and valley to the right remains relatively constant.

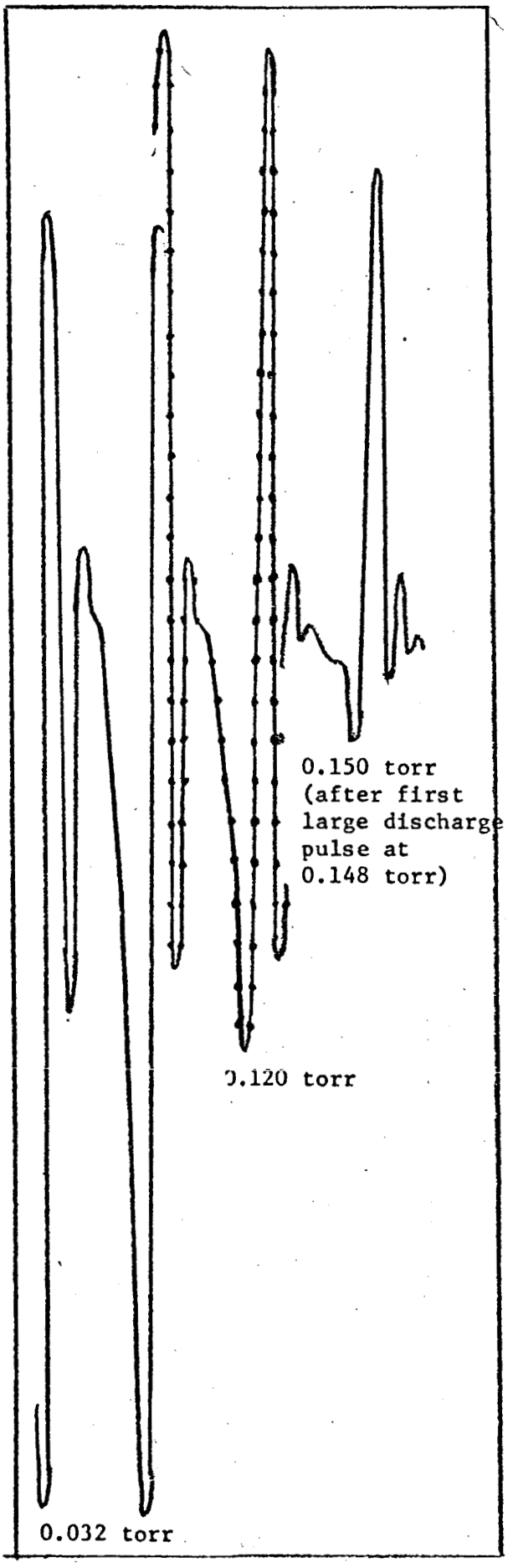

Figure 18. Run #3 charge distribution change with pressure increase from 0.032 torr to 0.120 torr is smooth. Change in distribution at 0.148 torr discharge pulse is a step increment.

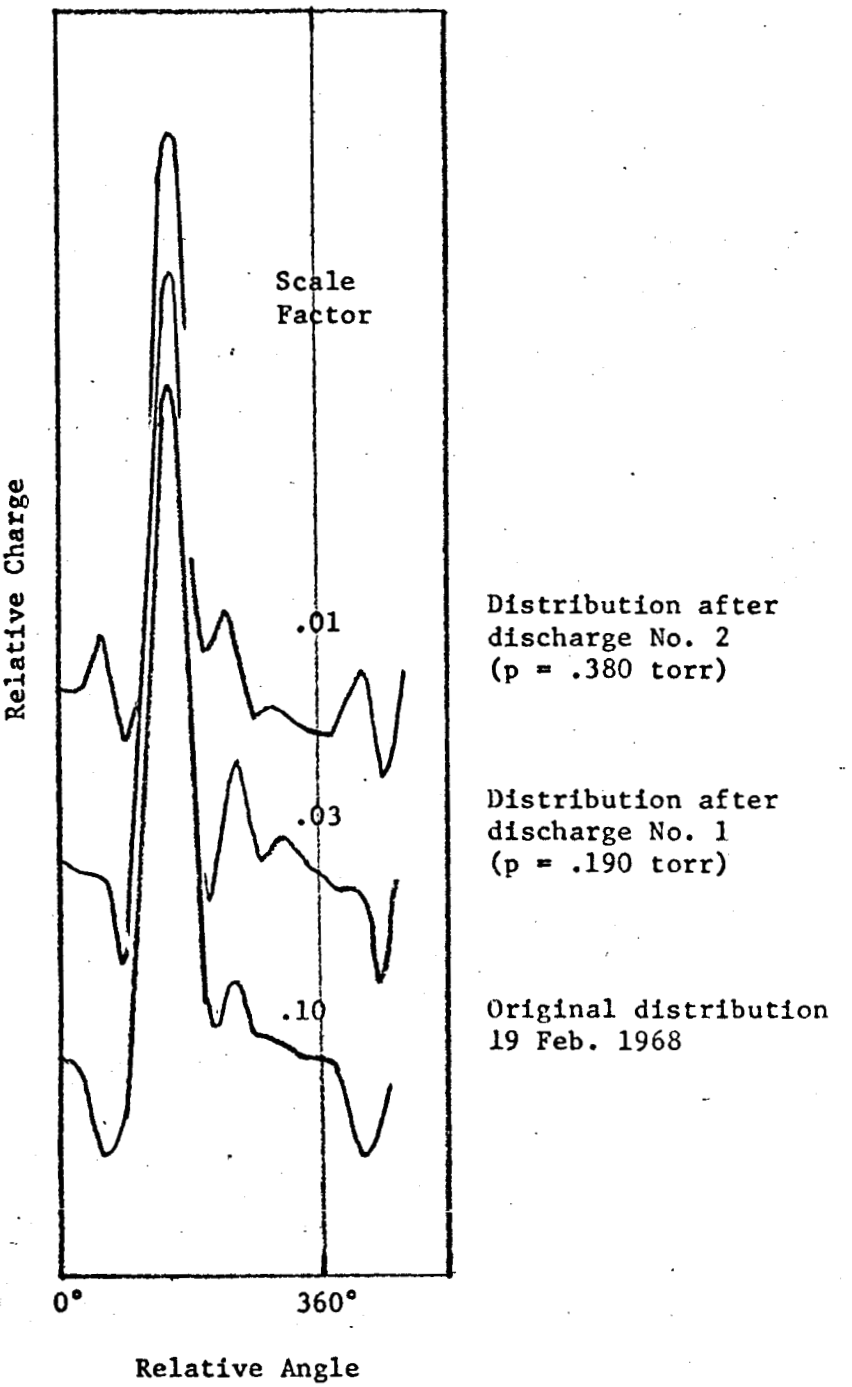

Figure 19. Charge distribution waveforms after discharge pulses compared with original distribution before touching surface with electrometer probe, Run #3.

pressure of 15 microns argon. This was done to see what effect such pressure would have on the adhesion and to make the time between sputtering and contact as short as possible, hence reducing re-oxidation. The findings of no detectable adhesion (adhesion less than 10^2 dynes) are in accord with expectations from the results of the surface charging studies. These showed that discharging of the surfaces could occur beginning at about 10-20 microns pressure. The findings also indicate that any atomic bonding between the clean metal and silicate surfaces makes a much smaller contribution to adhesion force, after touch contact, than the surface charging. Studies will be made of the contacting surfaces after removal from the vacuum system to see if there is any evidence of material transfer.

For the third run, pumping was initiated after the completion of sputtering. In order to reduce possible re-oxidation of the metal sample we pumpted for only five minutes before cleavage of the silicate. At that time the system pressure was down to 5×10^{-8} torr. Measureable adhesion was present. Due to observation problems it was not possible to determine whether a long range attractive force was present. However, on the basis of the previous two runs, and the surface charging experiments, it is felt that surface charging was probably the prime contributor. Further studies are required to prove this.

There are not sufficient data as yet to reach any conclusions concerning the effect of the metal surface state upon metal-silicate adhesion. However, it does appear as a distinct possibility that the only times when large adhesion will be present is when the silicate surface is clean and charged, the implication being that the charging produced by fracture (or cleavage) in ultrahigh vacuum may be the dominant adhesion producing mechanism.

3.2 Electrostatic Charging

Additional evidence was found in Run #3 (Figure 12) that gas adsorption is responsible for the initial rapid decrease in the charge anisotropy. That is, the factor of ten higher system pressure at cleavage for Run #3 over Run #2, with a corresponding increase in the rate of adsorption, shortened the time of decrease sufficiently to prevent observation.

Previously, the basic trend observed for the nonuniform charge distribution was a decrease with increasing time and pressure. However, after the initial decrease, when the probe contacted the surface, the charge difference increased during the next 22 days, Figure 17. This increase (Run #3) and the recovery upon reevacuating the sample of Run #2, Figure 2, are new observations.

Observation of the persistance of the angular relationship in the charge distribution when the cleavage direction was changed in the same crystal, Figure 14, strongly suggests that cleavage involving brittle fracture produces a surface electric charge distribution which depends mainly on bulk crystalline properties rather than the cleavage direction. Volume electrical resistivity is the main factor in the long term persistance of the charge distribution in these experiments. An immobile, volume distribution of charge is strongly suggested by: first, the charge recovery effects discussed above (thought to be surface phenomena) which reexpose volume charges to the probe (releasing electric field lines into the vacuum); and second, after discharging the secondary surface effects introduced by scraping the surface of the crystal with the probe (Figure 16), the original charge distribution is recovered (Figure 19).

In previous reports the origin of the apparent surface charge was attributed to complex electrical interactions between composition gradients, point defects,

and dislocations. For the orthoclase crystals used in Runs #1, #2 and #3, it was found that perthite structures were present, Figures 2, 3 and 4. These are small compared to the expected characteristic length for space charge in dielectric crystals. Therefore the internal polarization fields produced in this case, would be expected to be the result of gradients in the average composition, Figure 5, 6 and 7. This has been to a large degree verified by noting that the average distribution gradients of the potassium and silicon, Figures 8 and 9, in Run #1 are aligned with the observed lobe pattern for the charge. It should be noted that both are oriented relatively closely to the crystallographic axes. This is believed to be fortuitous in that the composition gradient-axes orientation is a function solely of crystal growth whereas the charge orientation results from the interaction between the concentration gradient charge distribution and the diectric coefficient ellipsoid of low symmetry crystals.

The discharge process is interesting in that the probe invariably goes positive. This would occur if the probe tip collects positive ions to neutralize a negative image charge at the probe tip. Another possibility is that the electric vector is parallel to the surface. (This is supported by the observation that discharge, when it can be distinguished, seems to occur preferentially when the probe is in a region in which the charge density is changing rapidly with the crystal angle).

4.0 FUTURE WORK

4.1 Silicate-Metal Adhesion

Work during the next quarter will consist of completing the series of runs on aluminum 2024, and proceeding to other metals. The final runs on the aluminum will consist of (1) mechanically abrading the surface and contacting it with

a contaminated silicate surface, and (2) mechanically abrading the surface and contacting it with a freshly cleaved silicate surface.

4.2 Electrostatic Charging

Upon the termination of Run #4 the cleavage faces from Runs #2, 3 and 4 will be examined photomicrographically (before and after defect etching) and with the electron microprobe, to obtain the dislocation and composition profiles. These will be compared to the charge distributions as was done for Run #1. Additionally, other silicate crystals will be studied in the same manner and increased emphasis will be placed upon determining the precise mechanisms responsible for the charge discharge and charge recovery.

Instrumentation-wise, the vacuum system will be rearranged to accommodate the new electrometer probe which is currently being fabricated. Also, the presently used Keithley 610B electrometer will be replaced by the much more sensitive 640, and a Phillips capacitance manometer will be utilized so that system pressure can be monitored up to atmospheric.

4.3 Effects of Various Gases

It has been found that the adhesion between freshly formed silicate surfaces (after touch contact) is due primarily if not entirely to electrostatic charging. Studies will begin shortly to determine the effects of various gases (such as H_2O, O_2, and CO_2) upon the adhesion. Since the adhesion force is a direct function of surface charging the effects of the various gases upon it will be determined by monitoring the electrostatic charge. These studies will provide information as to which gas has the greatest effect in reducing adhesion, as well as the amount required.